Barcelona '10

A022

3D Elastic Wavefield Inversion in the Time Domain

L. Guasch* (Imperial College London), M.R. Warner (Imperial College London), I. Stekl (Imperial College London) & A.P. Umpleby (Imperial College London)

SUMMARY

We have developed a 3D tomographic wavefield inversion code that solves the fully elastic wave equation in the time domain using finite differences. We show results of applying this elastic code to different synthetic 3D problems.

Introduction

Although acoustic wavefield inversion is widely used, a complete solution of the seismic inversion problem requires that we account properly for the physics of wave propagation, and so must include elastic effects. We have developed a 3D tomographic wavefield inversion code that incorporates the full elastic wave equation. The code uses explicit time-stepping by finite differences that are 4th order in space and 2nd order in time.

In terms of computational resource, the elastic code is an order of magnitude more demanding than the equivalent acoustic code. We have combined shared memory with distributed memory parallelisation using openMP and MPI respectively. Thus, we take advantage of the increasingly common multi-core architecture processors.

We calculate the parameter gradients for V_P and V_S by correlating the normal and shear stress wavefields respectively. The choice of parameters has a major impact on the convergence rate because each set of parameters corresponds to a different shape of the objective function. For transmission tomography, the choice of V_P and V_S narrows the minima in the solution space, thus we choose this model parameterisation. We show the results of applying this elastic code to a synthetic 3D problem, and compare the outcome to that obtained using a purely acoustic scheme for the tomography when the synthetic field data are fully elastic.

Elastic Wavefield Inversion

The goal of wavefield inversion is to match field data with synthetic generated data. The synthetic seismograms are created by discretising the space and solving the wave equation using numerical methods. When the misfit of the synthetic and field data is below an arbitrary threshold, the model used to generate the data is assumed to represent the real subsurface properties. Therefore, an accurate solver for the elastic wave equation is needed in combination with an iterative algorithm, which update the model parameters in order to minimise the misfit function.

Forward modelling

We calculate the synthetic data using a 4th order in space and 2nd order in time finite difference scheme, which solves the coupled systems of equations:

$$\rho \frac{\partial \mathbf{v}}{\partial t} = \nabla \boldsymbol{\tau}$$

$$\frac{\partial \boldsymbol{\tau}}{\partial t} = \mathbf{c} : \nabla \mathbf{v} \qquad (1)$$

where ρ is the density, $\mathbf{v}$ is the particle velocity vector, $\boldsymbol{\tau}$ is the stress tensor, $\mathbf{c}$ is the elastic tensor and **:** denotes the Frobenius inner product. The stencil is staggered both in space and time and it is a 3D version of the one developed by Levander (1988). The variables $\mathbf{v}$ and $\boldsymbol{\tau}$ are distributed spatially as shown in Figure 1 (staggered in space) and calculated at intermediate time-steps with respect to each other. Perfectly matched layers surround the model in order to prevent spurious reflections from the boundaries (Skarlatoudis *et al*, 2006).

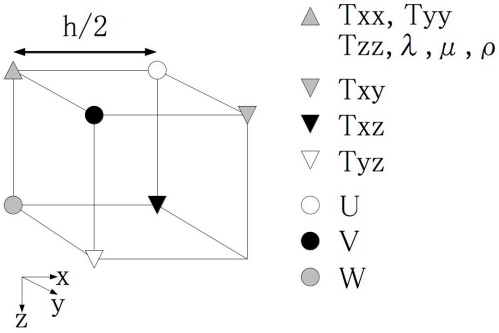

Figure 1 *3D unit cell used.* Tii *and* Tij (i,j ∈ {x,y,z}) *are the discrete normal and shear stresses respectively;* λ *and* μ *are the Lamé parameters;* U, V *and* W *are the discrete particle velocities in x, y and z directions.*

We speed up our modelling scheme by solving the FD equations in a sub-domain region around the source. We let this region grow as the wavefront evolves, until it reaches the model limits. Analogously, the information that can hit the receivers is confined in a shrinking box as time increases. The intersection of these two boxes defines the sub-domain where the wave equation is solved. Figure 2 shows two 2D slices in the YZ plane with a superimposed image of the acoustic and elastic wavefield calculated with our code.

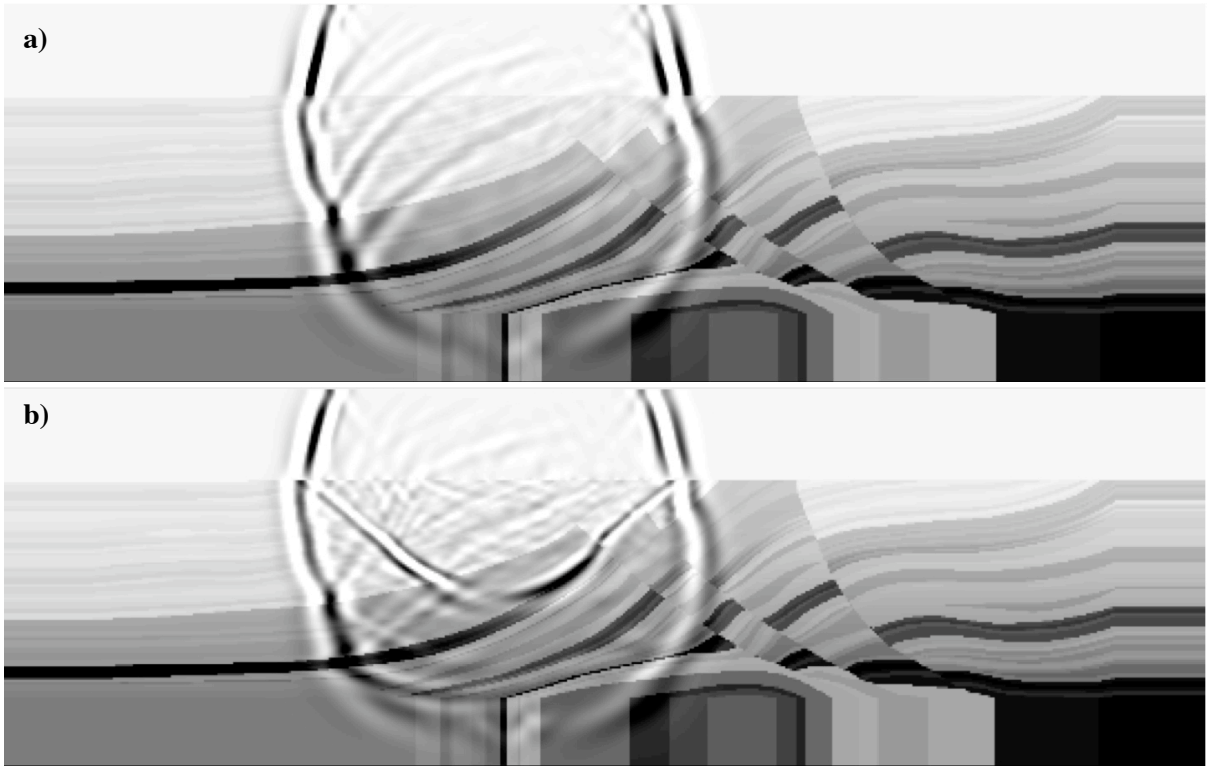

Figure 2 *Snapshots after 1.2 seconds showing the horizontal component of the particle velocity wavefield in a YZ slice of a 2.5D extension of the Marmousi model. In the acoustic case* **a)** *note the absence of the wavefront corresponding to an S-wave present in the elastic case* **b)**.

Inversion

The formulation of the elastic inverse problem was developed around 25 years ago (Tarantola, 1986) as a locally iterative linearised gradient descent method. It has only recently been applied to 3D problems due to its computational cost. The calculation of the Fréchet kernel is, nowadays, computationally unaffordable. Fortunately, Tarantola derived an alternative expression for the explicit

derivative of the wavefield with respect to the model parameters, which is based on the propagation backwards in time of the difference between the observed and modelled data (for the complete development see for example Mora, 1986). The correlation of this backpropagated wavefield and the forward modelled wavefield gives an expression of the gradient for each elastic parameter. Such approach has been used successfully in the acoustic case in both 2D (Pratt, 1999) and 3D (Warner *et al*, 2007).

The misfit function has different shapes depending on the parameterisation of the model. The choice of parameters affects the shape of such function, and therefore the convergence rate when we linearise it. We choose to update V_P and V_S instead of the Lamé parameters because the minima are narrower for wide-angle geometries (Mora, 1987). Due to our wave equation formulation, which solves for particle velocities and stresses, we derive expressions for the P- and S-wave gradients in terms of the stresses rather than particle displacements. Shipp and Singh (2002) developed an expression for the P-wave gradient in terms of the normal stresses, which we have extended to the S-wave case. The expressions of the gradient in terms of the Lamé parameters are of the form:

$$\delta\gamma = \int dt\left[\Omega^{\gamma}_{ijk}\vec{u}_j(\mathbf{x},t)\right]\left[\Omega^{\gamma}_{ijk}\bar{\Psi}_j(\mathbf{x},t)\right] \tag{2}$$

where $\delta\gamma$ represents the gradient for $\gamma \in \{\lambda,\mu,\rho\}$, $\vec{u}_j$ is the j^{th} component of the forward propagated particle displacement wavefield, $\bar{\Psi}_j$ is j^{th} component of the backpropagated residuals wavefield and Ω^{γ}_{ijk} is an operator with values:

$$\begin{aligned}
\Omega^{\rho}_{ijk} &= \sqrt{-1}\partial_t \\
\Omega^{\lambda}_{ijk} &= \sqrt{-1}\partial_j \\
\Omega^{\mu}_{ijk} &= \sqrt{\frac{-1}{2}}\left(\delta_{jk}\partial_i + \delta_{ji}\partial_k\right)
\end{aligned} \tag{3}$$

and the relation between $\{\lambda,\mu\}$ and $\{V_P,V_S\}$ gradients is given by:

$$\begin{aligned}
\delta V_P &= 2\rho V_P \delta\lambda \\
\delta V_S &= -4\rho V_P \delta\lambda + 2\rho V_S \delta\mu
\end{aligned} \tag{4}$$

where we dropped $\delta\rho$ because we keep the density constant through the inversion process.
Rewriting the system of equations (1) in terms of particle displacements instead of velocities gives us the following relationship between stresses and displacements (Einstein notation):

$$\begin{aligned}
\frac{1}{2(\lambda+\mu)}\tau_{ii} &= \frac{\partial u_j}{\partial j} \\
\frac{2-\delta_{ij}}{\delta_{ij}\lambda+\mu}\left(\tau_{ij}\right) &= \frac{\partial u_i}{\partial j} + \frac{\partial u_j}{\partial i}
\end{aligned} \tag{5}$$

with $i,j \in \{x,y,z\}$. Combining (4) and (5) it is possible to write the equations (2) in terms of stresses instead of particle displacements. As one may think intuitively, the correlation of the forward and backpropagated normal stresses provides the V_P gradient and the correlation of the shear stresses, the V_S gradient. The final gradient expressions are:

$$\begin{aligned}
\delta V_P &= \int dt\left(\vec{\tau}_{xx} + \vec{\tau}_{yy} + \vec{\tau}_{zz}\right)\left(\bar{\tau}_{xx} + \bar{\tau}_{yy} + \bar{\tau}_{zz}\right) \\
\delta V_S &= \int dt\left(\vec{\tau}_{xy} + \vec{\tau}_{xz} + \vec{\tau}_{yz}\right)\left(\bar{\tau}_{xy} + \bar{\tau}_{xz} + \bar{\tau}_{yz}\right)
\end{aligned} \tag{6}$$

Application to synthetic data

Two synthetic datasets were used to test the performance of our wavefield inversion scheme. The first was generated shooting and P- and S-waves in the XY and XZ planes of a cube and recording in the opposite faces. Figure 3a) shows the distribution of the anomalies in the seismic velocities. This model serves us as a benchmark to control the quality of the inverted data under different conditions. Figure 3b) shows the V_P gradient after the first iteration. T

The second model tested was a 2.5D version of the Marmousi model. We inverted this synthetic dataset using a smoothed true velocity and a Traveltime Tomography as starting models.

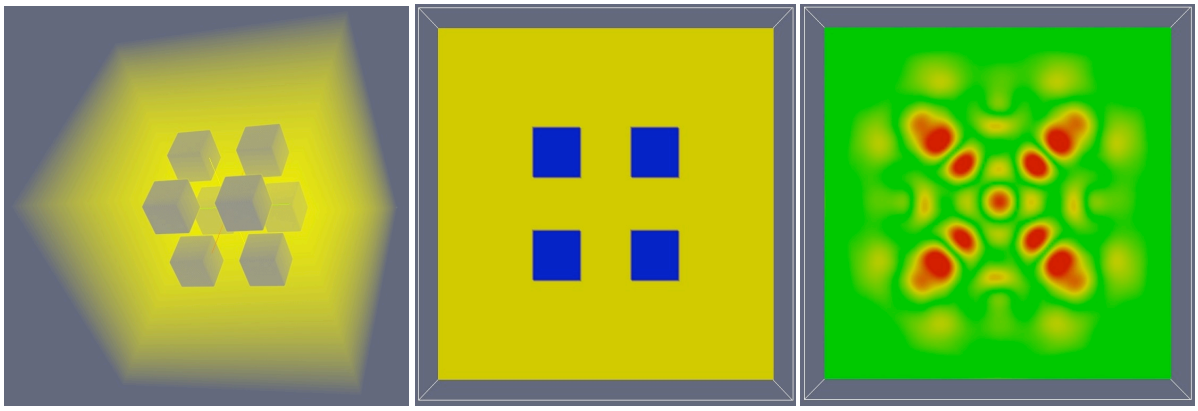

a) **b)** **c)**

Figure 3 **a)** *3D view of the true model the yellow area corresponds to 2500 m/s and the blue to 2625 m/s;* **b)** *2D slice of the true model* **a)***;* **c)** *Normalised Vp gradient after the first iteration.*

Conclusions

We have developed a wavefield inversion algorithm that successfully recovers the elastic properties of the subsurface. Shared and distributed memory parallelisation makes possible to tackle real sized 3D problems.

Acknowledgments

This work was sponsored by the FULLWAVE III consortium consisting of BIS, BG, BP, Chevron, CGGVeritas, ConocoPhillips, ENI, Maersk, Nexen, OHM, and Rio Tinto, under the ITF programme.

References

Levander, A.R., 1988. Fourth-order finite-difference P-SV seismograms, Geophysics, 53, 1425-1436

Skarlatoudis, A.A., Kristek, J., Moczo, P., Papazachos, C.B., 2006. Implementation of a non-splitting formulation of perfect matching layers in a 3D-4th order staggered-grid velocity-stress finite difference scheme, 1st ECEES, paper number 849

Tarantola, A., 1986. A strategy for nonlinear inversion of seismic reflection data, Geophysics, 51, 1893-1903

Mora, P., 1987. Nonlinear two-dimensional elastic inversion of multioffset seismic data, Geophysics, 52, 1211-1228

Pratt, G., 1999. Seismic waveform inversion in the frequency domain, part 1: Theory and verification in a physical scale model, Geophysics, 64, 888-901

Warner, M., Stekl, I., Umpleby, A., 2007. Full waveform seismic tomography-iterative forward modeling in 3D, 69th EAGE meeting, expanded abstract C, volume 25